Relativistic cross sections of electron-impact ionization of hydrogenic ions

Hsien-Chung Kao, Tien-Yow Kuo, Hsiang-Ping Yen, Ching-Ming Wei, and Keh-Ning Huang
Institute of Atomic and Molecular Sciences, Academia Sinica, P.O. Box 23-166, Taipei, Taiwan 10764, Republic of China
and Department of Physics, National Taiwan University, Taipei, Taiwan, 10764, Republic of China
(Received 24 October 1991)

Total and single-differential cross sections for electron-impact ionizaton are calculated in a relativistic formulation for ions in the hydrogen isoelectronic sequence: H I, He II, C VI, Ne X, Fe XXVI, and Ag XLVII. Transition amplitudes are evaluated in the two-potential distorted-wave approximation. Sets of different asymptotic charges are used to study the mutual screening of the primary and secondary electrons. Relativistic effects are investigated by taking the nonrelativistic limit and are found to increase the cross sections. Thomson's scaling law along the isoelectronic sequence is also studied.

PACS number(s): 34.80.Dp

I. INTRODUCTION

Cross sections of electron-impact ionization of highly charged ions are needed for the understanding of a wide variety of physical phenomena in high-temperature plasmas. A review of earlier works on electron-impact ionization of atoms was given by Rudge [1]. Experimental measurements of total cross sections for electron-ion collisions was surveyed by Dolder and Peart [2]. A more recent compilation of experimental and selected theoretical data was given by Tawara and Kato [3].

The electron-impact ionization of atomic hydrogen and hydrogenic ions had been studied by Burgess and Rudge [4] and by Rudge and Seaton [5]. The ionization cross sections for H I and He II were calculated in a Born-exchange approximation by Rudge and Schwartz [6]. Cross sections of electron-impact ionization for He II, C VI, Ne X, and Fe XXVI were computed by Younger [7,8] in several variants of the Coulomb-Born and distorted-wave approximations, where the exchange effects were taken into account by making the "maximum-interference" approximation. Other theoretical cross sections for hydrogenic ions were given, e.g., by Salop [9], by Banks and Boesten [10], by Kunc [11], and by Tsuji, Kotegawa, and Narumi [12]. Measurements of the ionization cross sections for H I were made by Fite and Brackmann [13], by Rothe *et al.* [14], and by McGowan and Clarke [15]. The ionization cross sections for He II were measured by Dolder, Harrison, and Thonemann [16], by Peart, Walton, and Thonemann [17], and by Defrance *et al.* [18]. Donets and Ovsyannikov [19] measured the ionization cross sections for C VI and Ne X.

Although there have been many theoretical studies on this topic, the results are not satisfactory. In many cases, relativistic effects are neglected; therefore, it is desirable to carry out a relativistic calculation. In this paper we will investigate the ionization cross sections of ions in the hydrogenic isoelectron sequence: H I, He II, C VI, Ne X, Fe XXVI, and Ag XLVII. The two-potential distorted-wave approximation is adopted to minimize the residual interaction. The results are compared with experiment and with other calculations. To show the sharing of the available kinetic energy, we also give the single-differential cross sections for H I and He II. Relativistic effects are studied by calculating the total cross sections in the nonrelativistic limit.

In Sec. II we will present the general theory of electron-impact ionization and the two-potential distorted-wave approximation. We carry out the angular decoupling of the transition matrix element and describe the numerical methods in Sec. III. In Sec. IV, present results are compared with those from other theories and with experiment.

II. THEORY

A. Kinematic analysis

In the electron-impact ionization processes, we denote the linear momentum and energy of the incident electron by $\mathbf{k}_i$ and E_i, respectively. Before the collision, the hydrogenic ion is in its ground state with only one electron. After the collision, the ion is deprived of its electron and becomes a bare nucleus. The two outgoing electrons are described by $(\mathbf{k}_p E_p)$ and $(\mathbf{k}_s E_s)$, where the primary electron is defined as the faster one, and the secondary electron as the slower one.

By energy conservation, we have

$$E_i + E_b = E_p + E_s \ , \tag{1}$$

where E_b is the energy of the bound electron. From the scattering theory, it follows that

$$\frac{d^3\sigma}{dE_s d\Omega_p d\Omega_s} = \frac{(2\pi)^4}{c^6}\left[\frac{k_p E_p k_s E_s E_i}{k_i}\right]|T_{fi}|^2 \ , \tag{2}$$

where T_{fi} denotes symbolically the transition matrix element. By integrating the triple-differential cross sections over Ω_p and Ω_s, we obtain the following expression for the single-differential cross section [20]:

$$\frac{d\sigma}{dE_s} = \frac{(2\pi)^3}{k_i^2(2j_b+1)}\overline{\sigma} \ , \tag{3}$$

where

$$\bar{\sigma}=\sum_{k_i,k_s,k_p,k_i,j} d_\alpha^2 \ . \tag{4}$$

Here the summation is over all possible channels, and the real amplitude d_α is defined by the reduced matrix element of the partial-wave amplitude in channel α, i.e.,

$$d_\alpha \exp(i\delta_\alpha)=i^{l_i-(l_p+l_s)}\exp[i(\sigma_{\kappa_p}+\sigma_{\kappa_s})] \times\langle \alpha^-(j_s j_p)J\|H_I\|(j_b j_i)J\rangle \ , \tag{5}$$

where H_I denotes symbolically the appropriate interaction.

The total cross sections can be calculated as

$$\sigma=\int_{mc^2}^{(E_i+E_b)/2}\frac{d\sigma}{dE_s}dE_s \ , \tag{6}$$

where mc^2 is the rest energy of the electron, and c is the speed of light.

B. Two-potential distorted-wave approximation

In our case, the total Hamiltonian H is assumed to be, in atomic units,

$$H=(c\alpha_1\cdot\mathbf{p}_1+c^2\beta_1)+(c\alpha_2\cdot\mathbf{p}_2+c^2\beta_2) -\frac{Z}{r_1}-\frac{Z}{r_2}+\frac{1}{r_{12}} \ , \tag{7}$$

where α_i and β_i are Dirac matrices, and the speed of light c equals the inverse of the fine-structure constant in atomic units. It can be separated in a physically meaningful way into two parts:

$$H=H_i+V_i \ , \tag{8}$$

where

$$H_i=(c\alpha_1\cdot\mathbf{p}_1+c^2\beta_1)+(c\alpha_2\cdot\mathbf{p}_2+c^2\beta_2)-\frac{Z}{r_2} \ , \tag{9}$$

$$V_i=-\frac{Z}{r_1}+\frac{1}{r_{12}} \ . \tag{10}$$

Here $\mathbf{r}_1$ and $\mathbf{r}_2$ refer to the spatial coordinates of the incident and bound electrons, respectively, before the collision and those of the primary and secondary electrons after the collision.

By considering antisymmetrization, the transition matrix element will have an exchange term in addition to the usual direct term. In the prior form, it is given by

$$T_{fi}=\langle \Psi_f^{(-)}|V_i|\Phi_i\rangle-\langle P\Psi_f^{(-)}|V_i|\Phi_i\rangle \ , \tag{11}$$

where P denotes the permutation of the two electrons.

In the two-potential formulation, the interaction potential may be split as

$$V_i=U_i+W_i. \tag{12}$$

Because in the initial state the incident electron is screened by the bound electron, we may well choose

$$U_i=-\frac{Z}{r_1}+v_i(r_1) \ , \tag{13}$$

$$W_i=\frac{1}{r_{12}}-v_i(r_1) \ . \tag{14}$$

Here v_i is the average potential due to the bound electron, i.e.,

$$v_i(r_1)=\left\langle \Phi_b(\mathbf{r}_2)\left|\frac{1}{r_{12}}\right|\Phi_b(\mathbf{r}_2)\right\rangle \ , \tag{15}$$

where $\Phi_b(\mathbf{r}_2)$ is the ground-state wave function. The potential U_i is taken to be the distorting potential for the incident electron. The distorted wave $\psi_i^{(+)}$ can then be expressed as

$$\psi_i^{(+)}=\chi_i^{(+)}(\mathbf{r}_1)\Phi_b(\mathbf{r}_2) \ , \tag{16}$$

where $\chi_i^{(+)}$ satisfies the following equation:

$$(c\alpha_1\cdot\mathbf{p}_1+c^2\beta_1+U_i-E_i)\chi_i^{(+)}(\mathbf{r}_1)=0 \ . \tag{17}$$

After some algebra, the transition matrix element (11) becomes

$$T_{fi}=\langle \Psi_f^{(-)}|W_i|\psi_i^{(+)}\rangle-\langle P\Psi_f^{(-)}|W_i|\psi_i^{(+)}\rangle \ . \tag{18}$$

To find an approximation to the final-state wave function Ψ_f^-, we choose the distorted final-state wave function as

$$\psi_f^{(-)}=\chi_p^{(-)}(\mathbf{r}_1)\chi_s^{(-)}(\mathbf{r}_2) \ , \tag{19}$$

where $\chi_p^{(-)}$ and $\chi_s^{(-)}$ satisfy the following equations:

$$(c\alpha_1\cdot\mathbf{p}_1+c^2\beta_1+U_p-E_p)\chi_p^{(-)}(\mathbf{r}_1)=0 \ , \tag{20}$$

$$(c\alpha_2\cdot\mathbf{p}_2+c^2\beta_2+U_s-E_s)\chi_s^{(-)}(\mathbf{r}_2)=0 \ . \tag{21}$$

The distorting potentials U_p and U_s for primary and secondary electrons, respectively, have three alternative choices for three different models used in the present calculation; they are summarized in Table I. Here TPDW stands for the relativistic two-potential distorted-wave formulation of this paper. In model TPDW01, the primary electron is completely screened by the secondary electron in the asymptotic region such that the primary electron is affected by an asymptotic charge of $Z-1$. The secondary electron is affected only by the Coulomb potential of the nucleus for an asymptotic charge of Z. For the hydrogen atom, the asymptotic charges Z_p and Z_s for the primary and secondary electrons, respectively, are 0 and 1 in model TPDW01. Similarly the asymptotic charges (Z_pZ_s) in models TPDW00 and TPDW11 are (00) and (11), respectively, for the hydrogen atom. At finite distances, the screening by the other electron is approximated by a potential due to the ground-state wave function, which is the same screening potential as that of the incident electron. Substituting $\Psi_f^{(-)}$ by $\psi_f^{(-)}$, we arrive at an approximate expression for the transition matrix element (18) as

TABLE I. Distorting potentials and asymptotic charges for the primary and secondary electrons in models TPDW01, TPDW00, and TPDW11.

	Distorting potential		Asymptotic charges	
Model	U_p	U_s	Z_p	Z_s
TPDW00	$-\frac{Z}{r_1}+v_i(r_1)$	$-\frac{Z}{r_2}+v_i(r_2)$	$Z-1$	$Z-1$
TPDW01	$-\frac{Z}{r_1}+v_i(r_1)$	$-\frac{Z}{r_2}$	$Z-1$	Z
TPDW11	$-\frac{Z}{r_1}$	$-\frac{Z}{r_2}$	Z	Z

$$T_{fi}=\left\langle\chi_p^{(-)}(\mathbf{r}_1)\chi_s^{(-)}(\mathbf{r}_2)\left|\frac{1}{r_{12}}-v_i(r_1)\right|\chi_i^{(+)}(\mathbf{r}_1)\Phi_b(\mathbf{r}_2)\right\rangle-\left\langle\chi_p^{(-)}(\mathbf{r}_2)\chi_s^{(-)}(\mathbf{r}_1)\left|\frac{1}{r_{12}}-v_i(r_1)\right|\chi_i^{(+)}(\mathbf{r}_1)\Phi_b(\mathbf{r}_2)\right\rangle . \tag{22}$$

III. NUMERICAL METHOD

To evaluate the transition matrix element (22), we first calculate the distorted-wave functions, whose partial waves are given in the general form

$$\chi_a=\frac{1}{r}\begin{bmatrix} G_a\Omega_{\kappa_a m_a} \\ iF_a\Omega_{-\kappa_a m_a}\end{bmatrix}, \tag{23}$$

where $a=i,p,s$, and G_a and F_a satisfy the radial Dirac equations with corresponding potentials U_a,

$$\frac{dG_a}{dr}=-\frac{\kappa_a}{r}G_a+\frac{1}{c}(E_a+c^2-U_a)F_a , \tag{24}$$

$$\frac{dF_a}{dr}=-\frac{1}{c}(E_a-c^2-U_a)G_a+\frac{\kappa_a}{r}F_a . \tag{25}$$

We now define the following notations:

$$W_{ac}(r)=G_aG_c+F_aF_c , \tag{26}$$

$$R_l(r_1,r_2)=r_<^l/r_>^{l+1} , \tag{27}$$

$$[j]=(2j+1)^{1/2} ,$$

$$\langle W_{ac}V\rangle=\int_0^\infty dr\, W_{ac}(r)V(r) , \tag{28}$$

$$\langle W_{ac}R_lW_{bd}\rangle^{\text{even}}=\pi(l_all_c)\pi(l_bll_d)\times\int\int_0^\infty dr_1dr_2W_{ac}(r_1)R_l(r_1,r_2)\times W_{bd}(r_2) \tag{29}$$

with the parity function

$$\pi(l_all_\beta)=\begin{cases}1, & l_\alpha+l+l_\beta=\text{even}\\ 0, & l_\alpha+l+l_\beta=\text{odd}\end{cases} .$$

Using a graphical method [21], we can express the real partial-wave amplitude d_α in terms of the above notations as

$$d_\alpha=\left\langle\frac{1}{r_{12}}\right\rangle_d-\langle v_i\rangle_d-\left\langle\frac{1}{r_{12}}\right\rangle_e+\langle v_i\rangle_e , \tag{30}$$

where

$$\langle v_i\rangle_d=\{Jj_pj_s\}\langle W_{sb}\rangle\langle W_{pi}v_i\rangle , \tag{31}$$

$$\langle v_i\rangle_e=(-1)^{J+j_p+j_s}\{Jj_pj_s\}\langle W_{pb}\rangle\langle W_{si}v_i\rangle , \tag{32}$$

$$\left\langle\frac{1}{r_{12}}\right\rangle_d=\sum_l(-1)^{J+j_p+j_i}[j_pj_sj_ij_b]\begin{Bmatrix}j_p & j_s & J\\ j_b & j_i & l\end{Bmatrix}\begin{bmatrix}j_p & l & j_i\\ \frac12 & 0 & -\frac12\end{bmatrix}\begin{bmatrix}j_s & l & j_b\\ \frac12 & 0 & -\frac12\end{bmatrix}\langle W_{pi}R_lW_{sb}\rangle_{\text{even}} , \tag{33}$$

$$\left\langle\frac{1}{r_{12}}\right\rangle_e=\sum_l(-1)^{j_p-j_i}[j_pj_sj_ij_b]\begin{Bmatrix}j_s & j_p & J\\ j_b & j_i & l\end{Bmatrix}\begin{bmatrix}j_s & l & j_i\\ \frac12 & 0 & -\frac12\end{bmatrix}\begin{bmatrix}j_p & l & j_b\\ \frac12 & 0 & -\frac12\end{bmatrix}\langle W_{si}R_lW_{pb}\rangle_{\text{even}} . \tag{34}$$

Here, notation for $3n$-j coefficients has been used [21,22].

To study the mutual screening between the primary and secondary electrons, we have calculated the amplitudes d_α for different choices of distorting potentials shown in Table I. To show the relativistic effects, we also calculate the nonrelativistic cross sections by letting the speed of light c go to infinity. In practice, we set c to be 10^9 a.u.

IV. RESULTS AND DISCUSSION

To compare single-differential and total cross sections of different ions, we use the threshold energy units $u_i=(E_i-c^2)/I$, $u_p=(E_p-c^2)/I$, and $u_s=(E_s-c^2)/I$ measured with respect to the rest energy of the electron and reduced cross sections defined as

$$\left[\frac{d\sigma}{dE_s}\right]_{\text{reduced}}=\left[\frac{I}{I_H}\right]^3\frac{d\sigma}{dE_s}=Z^6\frac{d\sigma}{dE_s},$$

$$\sigma_{\text{reduced}}=\left[\frac{I}{I_H}\right]^2\sigma=Z^4\sigma .$$

Here I denotes the ionization potential of the particular ion in consideration, and I_H that of the hydrogen atom. We have calculated the single-differential cross sections for H I and He II at $u_i=1.25$ and 10.0, the total cross sections for H I, He II, C VI, Ne X, Fe XXVI, and Ag XLVII with u_i ranging from 1.125 to 10, and the total cross sections in the nonrelativistic limit.

In Fig. 1 we present the single-differential cross section for H I at $u_i=1.25$. The TPDW00 curve has a maximum in the low-u_s region because the secondary electron in the TPDW00 model is not affected by a long-range Coulomb potential, i.e., $Z_s=0$. The constancy of the TPDW11 curve is due to the fact that $Z_p\neq 0$ and $Z_s\neq 0$. It is apparent that at low incident energies the single-differential cross section depends strongly on both asymptotic charges Z_p and Z_s.

In Fig. 2 we present the single-differential cross section for H I at $u_i=10$. While the TPDW01 and TPDW11 curves come close together, they are quite different from the TPDW00 curve. This can be understood from the properties of Coulomb wave functions. Although the distorted waves $\chi_i^{(+)}$, $\chi_p^{(-)}$, and $\chi_s^{(-)}$, experience a pure Coulomb potential as well as a short-range potential, the following properties of Coulomb wave functions still apply. The Coulomb wave function depends on Z only through the parameter Z/k; therefore, it is insensitive to changes in Z when the momentum k is high. At high incident energies, the momentum of the primary electron is also high, and this makes the single-differential cross section depend weakly on Z_p. Consequently, the different asymptotic charges of the primary electron in the TPDW01 and TPDW11 models do not result in significantly different cross sections at high incident energies. The peak features in the TPDW00 curve is again due to the fact that $Z_s=0$. We also note that the total cross section comes mainly from the low-u_s region. In other words, an uneven sharing of the available kinetic energy (u_i-1) is more favorable at high incident energies.

In Fig. 3 the single-differential cross section for He II at $u_i=1.25$ is displayed. The three flat curves reflect the fact that for all three models, TPDW11, TPDW01, and TPDW00, both the primary and secondary electrons are affected by a long-range Coulomb potential, i.e., $Z_p\neq 0$ and $Z_s\neq 0$. This is similar to the TPDW11 curve for H I at $u_i=1.25$. An example of high incident energy is given in Fig. 4 for He II at $u_i=10$. All three curves decrease monotonically because $Z_s\neq 0$, similar to the TPDW01

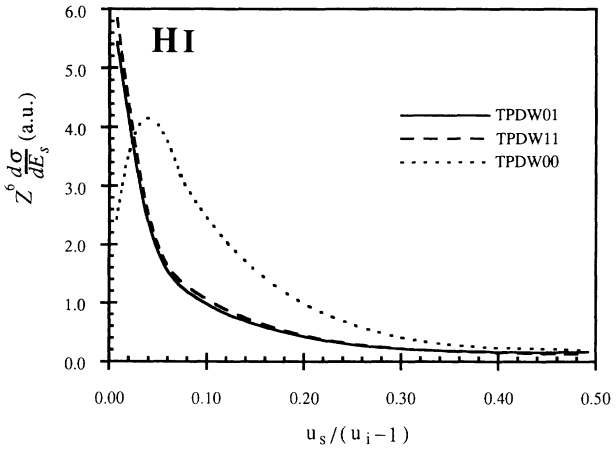

FIG. 2. Reduced single-differential cross sections (in a.u.) for H I at the incident energy $u_i=10$ (in threshold energy units).

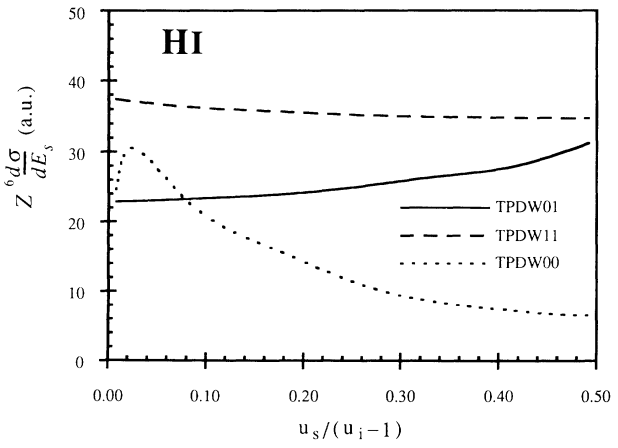

FIG. 1. Reduced single-differential cross sections (in a.u.) for H I at the incident energy $u_i=1.25$ (in threshold energy units).

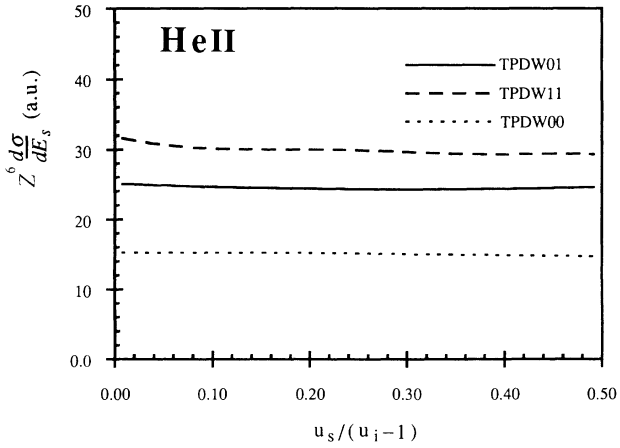

FIG. 3. Reduced single-differential cross sections (in a.u.) for H II at the incident energy $u_i=1.25$ (in threshold energy units).

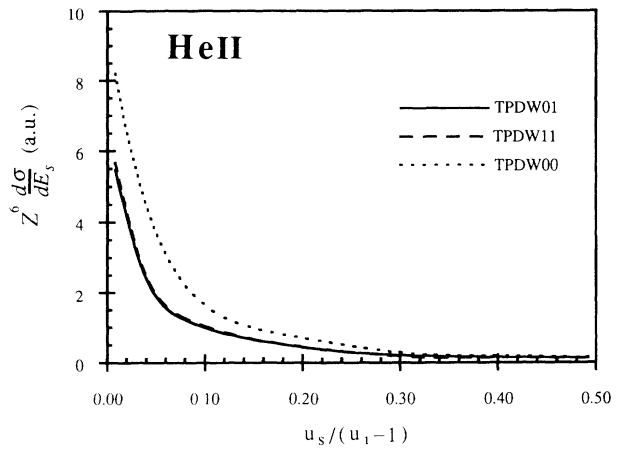

FIG. 4. Reduced single-differential cross sections (in a.u.) for H II at the incident energy $u_i = 10$ (in threshold energy units).

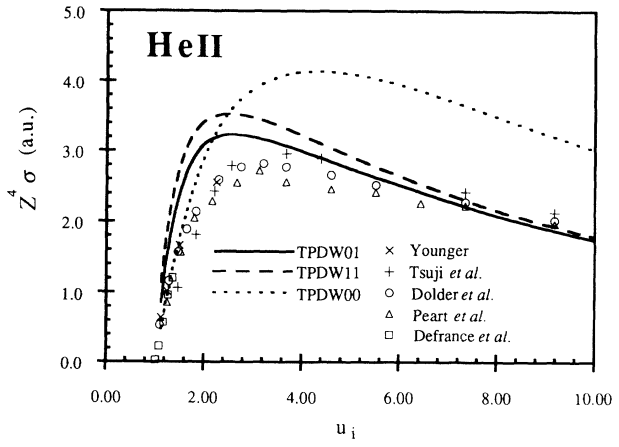

FIG. 6. Reduced total cross sections in (a.u.) for He II.

and TPDW11 curves in the H I case.

As a general conclusion, when both the primary and secondary electrons are affected by a long-range Coulomb potential, the single-differential cross section is nearly constant at low incident energies and decreases sharply with the secondary-electron energy at high incident energies. The physical picture is as follows. At low incident energies, all possible sharings of the available kinetic energy among the primary and secondary electrons are equally probable. As the incident energy increases, the collision becomes more likely to end up with an uneven sharing of the energy, i.e., high primary-electron energy and low secondary-electron energy. Another observation is that at high incident energies, the single-differential cross section depends strongly on the asymptotic charge of the secondary electron but weakly on that of the primary electron. Furthermore, as can be seen from Figs. 2 and 4, the total cross section at high incident energies comes predominantly from the low secondary-electron energy part of the single-differential cross section. All these conclusions can be explained qualitatively from the properties of Coulomb wave functions.

In Fig. 5 we show the total cross sections for H I and compare them with the theoretical results of Rudge and Schwartz [6] and with the experimental data of Fite and Brackmann [13], Rothe *et al.* [14], and McGowan and Clarke [15]. The TPDW00 curve is in good agreement with experiment at low incident energies, while the TPDW01 and TPDW11 curves give better agreement at high incident energies. At low incident energies, the available kinetic energies of the primary and secondary electrons are low. As a result, they are both strongly screened by each other so that the TPDW00 gives better results. As far as the total cross section is concerned, the TPDW00 seems to provide a practical model at low incident energies without a sophisticated treatment of the asymptotic charges. At high incident energies because the primary electron is likely to have a much higher velocity and to leave the collision region much sooner, the secondary electron is not screened. This makes both the TPDW01 and TPDW11 better models at high u_i.

In Fig. 6 we display the total cross sections for He II, compared with results from theoretical studies of Tsuji *et al.* [12] and Younger [7] and from experiments by Dolder *et al.* [16], Peart *et al.* [17], and Defrance *et al.*

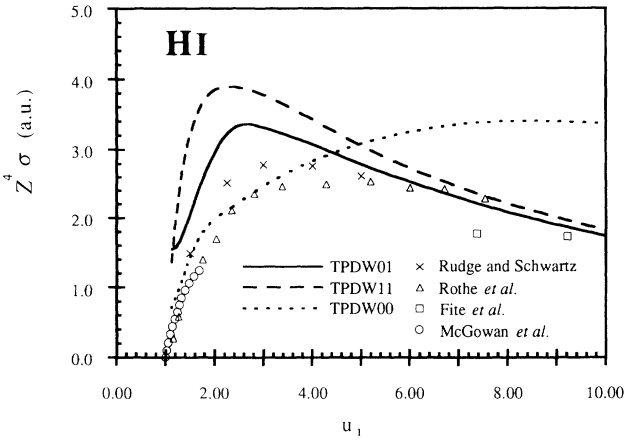

FIG. 5. Reduced total cross sections in (a.u.) for H I.

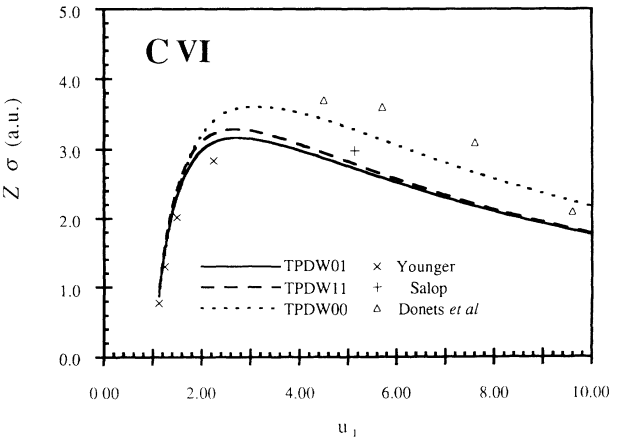

FIG. 7. Reduced total cross sections in (a.u.) for C VI.

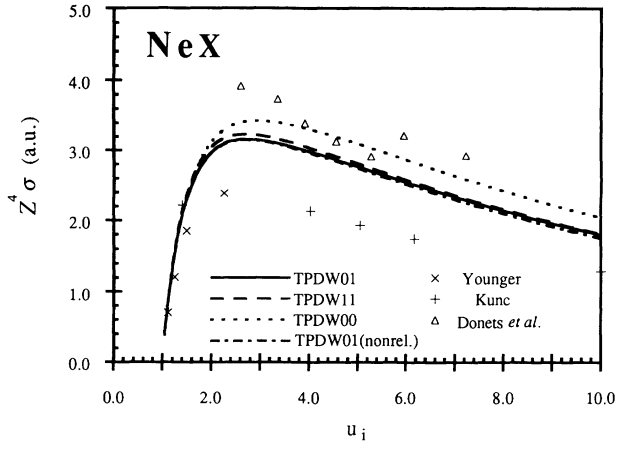

FIG. 8. Reduced total cross sections in (a.u.) for Ne X.

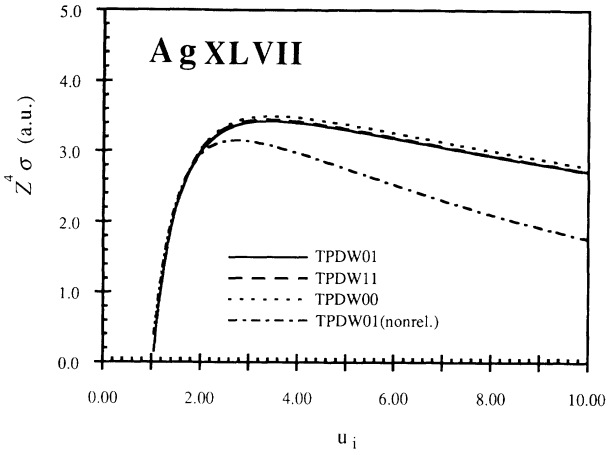

FIG. 10. Reduced total cross sections in (a.u.) for Ag XLVII.

[18]. Like the H I cases the TPDW00 results are in good agreement with experiment when u_i is low, and the TPDW01 gives better results at high u_i. As expected, the TPDW01 and TPDW11 results come close together. In Fig. 7 the present results for C VI are compared with the theoretical results of Younger [7] and Salop [9], and with the experimental results by Donets and Ovsyannikov [19]. Here further experimental studies are needed. Relativistic effects are still negligible for C VI. In Fig. 8 comparisons for Ne X are shown between our results, the theoretical calculations of Younger [7] and Kunc [11], and the experimental data of Donets and Ovsyannikov [19]. Similar to the comparison for C VI, the experimental results seem too large. The nonrelativistic TPDW01 curve is also presented in Fig. 8 and is slightly lower than the relativistic TPDW01 curve at high incident energies. In Fig. 9 we show the total cross sections for Fe XXVI and compare them with the isoelectronic parametrization results of Younger [8]. The TPDW01 and TPDW11 curves are almost indistinguishable. Younger's results are smaller than ours for all energies considered. The neglect of relativistic effects, the approximated treatment of exchange effects, and the omission of the matrix elements involving the distorting potential v_i in Younger's formulation probably account for the major part of the discrepancy. This discrepancy will be discussed further when we study the systematic trend along the hydrogen isoelectronic sequence. In Fig. 10 the total cross sections for Ag XLVII are displayed. Because of high nuclear charge Z, there is not much difference among the three models.

To study the systematics of total cross sections of electron-impact ionization along the hydrogen isoelectronic sequence, we plot TPDW01 results for all ions in Fig. 11. All curves seem to follow a universal trend, rising sharply at the threshold and decreasing gradually after about $u_i=2.6$. This universal trend is more apparent for nonrelativistic cross sections which are presented in Fig. 12. For ions after C VI, the nonrelativistic TPDW01 curves are indistinguishable from each other such that they form a universal curve. Here Thomson's scaling law [23] manifests itself in the

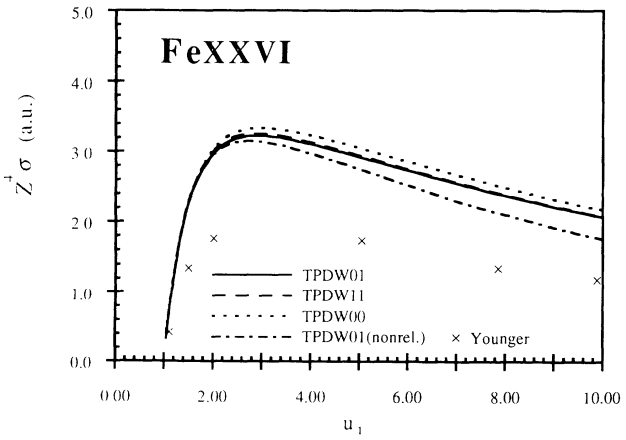

FIG. 9. Reduced total cross sections in (a.u.) for Fe XXVI.

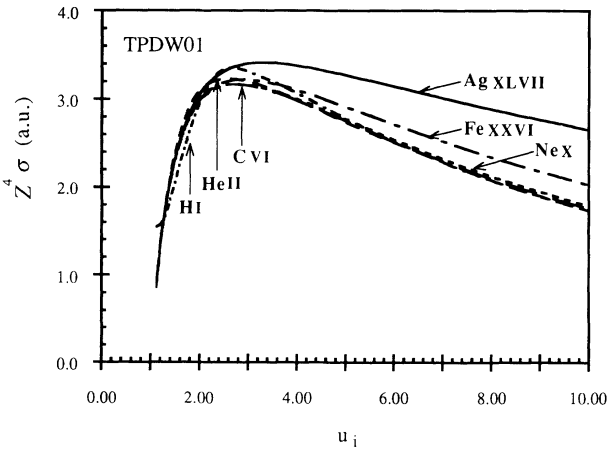

FIG. 11. Reduced total cross sections (in a.u.) in model TPDW01 for H I, He II, C VI, Ne X, Fe XXVI, and Ag XLVII.

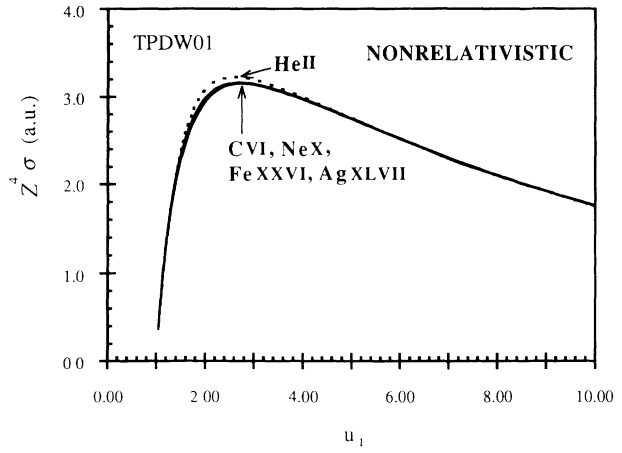

FIG. 12. Nonrelativistic reduced total cross sections (in a.u.) in model TPDW01 for He II, C VI, Ne X, Fe XXVI, and Ag XLVII.

quantum-mechanical case. In this connection, Younger's results for different ions do not form a universal curve. The deviation of the H I curve from the universal curve is due to the relative importance of the short-range potential. For clarity, the H I curve is not plotted in Fig. 12. The obvious deviations of the relativistic curves for Fe XXVI and Ag XLVII from the universal curve are due to the relativistic effects.

Starting from a relativistic formulation and considering antisymmetrization, we arrive at an exact expression for the transition matrix element of electron-impact ionization. This transition matrix element is then reduced in the two-potential distorted-wave formalism. Finally, the distorted-wave approximation is made for the final-state wave function. Three models are used for the distorting potentials for the primary and secondary electrons. Model TPDW00, in which the primary and secondary electrons are completely screened by each other in the asymptotic region, provides better agreement with experiment at low incident energies. Model TPDW01, in which only the primary electron is completely screened by the secondary electron, gives better results at high incident energies. Because the total cross sections at high incident energies come predominantly from the low secondary-electron energy region and because the cross section is insensitive to the asymptotic charge of the primary electron, models TPDW01 and TPDW11 yield similar results at high incident energies. Despite strong continuum correlations between the primary and secondary electrons at low incident energies, our predictions of the total cross sections of electron-impact ionization for ions in the hydrogen isoelectronic sequence are generally in good agreement with experiment.

ACKNOWLEDGMENT

This work was supported in part by the National Science Council of the Republic of China.

[1] M. R. H. Rudge, Rev. Mod. Phys. **4**, 546 (1968).
[2] K. T. Dolder and B. Peart, Rep. Prog. Phys. **39**, 693 (1976).
[3] H. Tawara and T. Kato, At. Data Nucl. Data Tables **36**, 167 (1987).
[4] A. Burgess and M. R. H. Rudge, Proc. R. Soc. London Ser. A **273**, 372 (1963).
[5] M. R. H. Rudge and M. J. Seaton, Proc. R. Soc. London Ser. A **283**, 262 (1965).
[6] M. R. H. Rudge and S. B. Schwartz, Proc. R. Soc. London **88**, 563 (1966).
[7] S. M. Younger, Phys. Rev. A **22**, 111 (1980).
[8] S. M. Younger, J. Quant. Spectrosc. Radiat. Transfer **27**, 541 (1982).
[9] A. Salop, Phys. Rev. A **14**, 2095 (1976).
[10] D. Banks and L. G. J. Boesten, J. Phys. B **11**, 2209 (1978).
[11] J. Kunc, J. Phys. B **13**, 587 (1980).
[12] A. Tsuji, H. Kotegawa, and H. Narumi, J. Phys. Soc. Jpn. **48**, 2026 (1980).
[13] W. L. Fite and R. T. Brackmann, Phys. Rev. **112**, 1141 (1958).
[14] E. W. Rothe, L. L. Marino, R. H. Neynaber, and S. M. Trujillo, Phys. Rev. **125**, 582 (1962).
[15] J. W. McGowan and E. M. Clarke, Phys. Rev. **167**, 43 (1968).
[16] K. T. Dolder, M. F. A. Harrison, and P. C. Thonemann, Proc. R. Soc. London, Ser. A **264**, 367 (1961).
[17] B. Peart, D. S. Walton, and P. C. Thonemann, J. Phys. B **2**, 1347 (1969).
[18] P. Defrance, F. Brouillard, W. Claeys, and G. Van Wassenhove, J. Phys. B **14**, 103 (1981).
[19] E. D. Donets and V. P. Ovsyannikov, Zh. Eksp. Teor. Fiz. **80**, 916 (1981) [Sov. Phys. JETP **53**, 466 (1981)].
[20] K.-N. Huang, Phys. Rev. A **28**, 1869 (1983).
[21] K.-N. Huang, Rev. Mod. Phys. **53**, 215 (1979).
[22] A. R. Edmonds, *Angular Momentum in Quantum Mechanics* (Princeton University, Princeton, NJ, 1957).
[23] J. J. Thomson, Philos. Mag. **23**, 449 (1912).